Catalysis Today 156 (2010) 216–222

Contents lists available at ScienceDirect

Catalysis Today

journal homepage: www.elsevier.com/locate/cattod

Catalytic membrane materials with a hierarchical porosity and their performance in total oxidation of propene

C. Yacou[a], A. Ayral[a,*], A. Giroir-Fendler[b], A. Baylet[b], A. Julbe[a]

[a] Institut Européen des Membranes, UMR 5635 CNRS-ENSCM-UM2, Université Montpellier 2, cc047, Place Eugène Bataillon, F-34095 Montpellier Cedex 5, France
[b] Institut de Recherches sur la Catalyse et l'Environnement de Lyon (IRCELYON), UMR 5256 CNRS - Université Lyon 1, 2, av. A. Einstein, 69626 Villeurbanne Cedex, France

ARTICLE INFO

Article history:
Available online 18 May 2010

Keywords:
Hierarchical membranes
SiO_2
SiO_2–TiO_2
Pt nanoparticles
Catalytic membrane
Membrane contactor
Propene oxidation

ABSTRACT

Pt nanoparticles (Pt-NPs) dispersed in either SiO_2 or SiO_2–TiO_2 hierarchical matrix were investigated for the total oxidation of propene as a typical volatile organic compound. The proposed scalable synthesis method, based on a "one pot" sol–gel pathway enables the encapsulation of isolated Pt-NPs mainly in the organised mesopores and guarantees their accessibility through the connected micropores of the oxide walls. The accessibility and stability of the Pt-NPs into this complex nanostructure were specially studied in this work. Pt–SiO_2 membrane materials with 1.7 wt% Pt revealed very efficient catalyst for the combustion of propene, with a light-off temperature lower that 110 °C. Interestingly, thermal treatments of these materials up to 850 °C do not destroy their catalytic activity thanks to the limited thermal growth of Pt-NPs within the hierarchical structure, and in spite of a strong reduction of their specific surface area. SiO_2–TiO_2 materials with 20 mol% SiO_2 also revealed an attractive hierarchical matrix for dispersing efficiently the Pt-NPs and performing the oxidation reaction below 200 °C.

1. Introduction

Emerging membrane applications involving the treatment of gases or vapors at high temperature require defect-free microporous membranes exhibiting both high thermal and chemical stability, and catalytic activity. Ceramic membranes with advanced properties and high reliability have great potential for membrane reactor applications [1] and new ceramic membrane designs can be advantageously considered [2]. Among the recent developments, ceramic membranes coupling a hierarchical porosity with an additional functionality deserve a great deal of attention.

Hierarchical membrane materials were developed in our group by a scalable processing sol–gel method [3]. As shown in Fig. 1, such materials can integrate three porosity levels: isolated macropores and mesopores embedded in a continuous microporous inorganic oxide phase. An additional functionality can be provided by dispersing, e.g. noble metal nanoparticles (NPs) in the mesopores while the macropores ensure a high permeability for the membrane. The membrane cut-off is defined by the microporous continuous solid phase.

One important potential advantage of such membranes is the substantial simplification of the preparation procedure for microporous ceramic membranes [4]. Indeed the deposition of good quality microporous layers usually requires a smooth mesoporous intermediate layer which moreover limits the whole membrane permeance. In the case of hierarchical membranes, formulated sols can be directly coated on a macroporous tubular support. Furthermore, the relatively large thickness of the resulting membranes limits the impact of potential top-surface defects in the continuous microporous phase. Finally, the possibility to disperse nanoparticles in the non-connected mesopores has great potential for stabilising highly reactive catalytic sites in a highly porous ceramic matrix.

Recently many nanostructured mesoporous oxides with high surface areas and uniform pore size distributions have been used as supports for multiple catalyst applications [5–7]. Their high surface areas and pore volumes are real assets to improve various catalytic reactions and adsorption/separation performance.

On the other hand, the increasing environmental awareness has prompted the emergence of stricter regulations covering automobile and industrial activities. Among these, the reduction of volatile organic compounds (VOCs) like propene should be important because these molecules present important photochemical ozone creativity potential (POCP) [8]. The catalytic oxidation of these pollutants to carbon dioxide and water has been identified as one of the most efficient ways to destroy VOCs at low concentrations and to meet increasingly environmental regulations [9]. The practical applications of the catalytic combustion process require heating large amounts of gas containing low concentrations of VOCs in order to reach the oxidation temperature. Therefore, highly active catalysts at low temperatures with a facil-

* Corresponding author. Tel.: +33 4 67 14 91 43; fax: +33 4 67 14 91 19.
E-mail address: andre.ayral@iemm.univ-montp2.fr (A. Ayral).

0920-5861/$ – see front matter © 2010 Elsevier B.V. All rights reserved.
doi:10.1016/j.cattod.2010.04.025

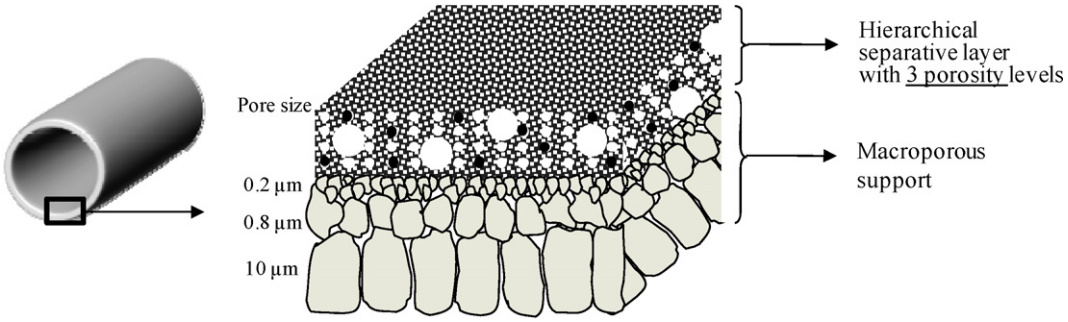

Fig. 1. Schematic representation of a supported multifunctional ceramic tubular membrane with 3 porosity levels and dispersed metal nanoparticles inside the mesopores.

itated access of the reactant to the active sites are specifically required.

The present work deals with silica-based hierarchical porous membranes containing dispersed Pt nanoparticles (Pt-NPs). After a short description of the membrane structure, and of gas permeance results, the catalytic performance of the membrane material for the oxidation of propene will be reported and discussed. We focused on both the accessibility and the stability of the dispersed Pt-NPs embedded in the mesoporous phase of the hierarchical structure obtained by a very simple one pot microwaves-assisted sol–gel route. Indeed the stability of NPs is a well debated requirement in relation to catalytic processes due to deactivation caused by metal sintering [10,11]. In order to estimate the influence of the support used for stabilizing the Pt-NPs on their catalytic performance, series of Pt/TiO_2–SiO_2 hierarchical composites materials with 20 mol% SiO_2 have been also investigated. This type of material is an attractive example of catalysts in which the catalytic properties of the metal component can be potentially improved by its interaction with the active semi-conducting oxide support [12]. Such nanocomposite oxide matrix also possesses intrinsic photocatalytic activity [13].

2. Experimental procedure

2.1. Materials

For pure SiO_2 membranes, the starting hybrid sol was synthesized by following the "one pot" protocol previously described in [14]. A TEOS-derived silica sol was mixed with a triblock copolymer (Pluronic F68). The Pt precursor, $H_2PtCl_6{\cdot}6H_2O$, previously dissolved in ethylene glycol (EG) was then poured into the hybrid sol. The metal precursor was reduced within few seconds by irradiation in a domestic microwave (MW) oven. Polystyrene (PS) latex spheres were finally added as macropore formers, yielding a complex stable suspension.

For the SiO_2–TiO_2 membranes, a TEOS-derived sol prepared with HCl, EG, F68 and $H_2PtCl_6{\cdot}6H_2O$ was first irradiated in the domestic MW oven (sol A). The molar ratios were $TEOS:EtOH:H_2O:F68:EG:H_2PtCl_6 = 1:3.8:2.6:8.7 \times 10^{-3}:6.2:3.5 \times 10^{-3}$. After cooling, the sol was slowly poured in an anatase hydrosol (sol B) obtained by acidic hydrolysis of Ti isopropoxide. The sol synthesis conditions were detailed in [15]. The PS latex spheres and an additional quantity of F68 were finally added in the mixture. The inserted amount of the F68 and the PS in the dried materials corresponds to a volume fraction of 77% and 45%, respectively. A sol corresponding to a final oxide composition with 80% molar content of TiO_2 and 20% molar content of SiO_2 was prepared. The flowchart of the synthesis procedure is shown in Fig. 2.

A series of hierarchical SiO_2 and SiO_2–TiO_2 membranes containing Pt-NPs were prepared by slip-casting sols on the internal surface of asymmetric α-alumina tubular supports (Pall-Exekia with 200 nm mean pore size in the top-layer). The derived supported layers were first thermally treated for several hours at either 175 °C or 150 °C (for SiO_2: dwells at 100 °C, 150 °C and 175 °C with a heating rate of 0.1 °C min^{-1}, dwell time of 6 h and final natural cooling; for SiO_2–TiO_2: dwells at 60 °C, 100 °C and 150 °C with a heating rate of 0.1 °C min^{-1}, dwell time of 6 h and final natural cooling). Finally, materials were all calcined in air at 450 °C for 2 h in order to operate a gentle thermal degradation of the organic porogen phases. Equivalent powders were also prepared by pouring sols on Teflon™ sheets.

Pure SiO_2 hierarchical membranes containing either 0.18 wt% Pt, 1 wt% Pt or 1.7 wt% Pt will be later labelled $HS_{pure}Pt0.18$, $HS_{pure}Pt1$, and $HS_{pure}Pt1.7$, respectively. Hierarchical SiO_2–TiO_2 membranes containing 0.18 wt% Pt and 1.7 wt% Pt will be later labelled $HS_{mix}Pt0.18$ and $HS_{mix}Pt1.7$, respectively.

In order to evaluate the thermal stability of the catalytic activity, the performance of $HS_{pure}Pt1.7$ powders has been also measured after a thermal treatment in air at either 650 °C or 850 °C for 2 h.

2.2. Material characterisation

Transmission electron microscopy (TEM) images were recorded on a JEOL-JEM 2010. The samples obtained by scratching the films from the substrates were suspended in ethanol, followed by 10 min sonication in an ultrasonic bath. Carbon-coated copper grids were used as sample holders.

Wide-angle XRD (WXRD) patterns of the equivalent powders were collected using an X'pert-Pro PanAnalytical diffractometer

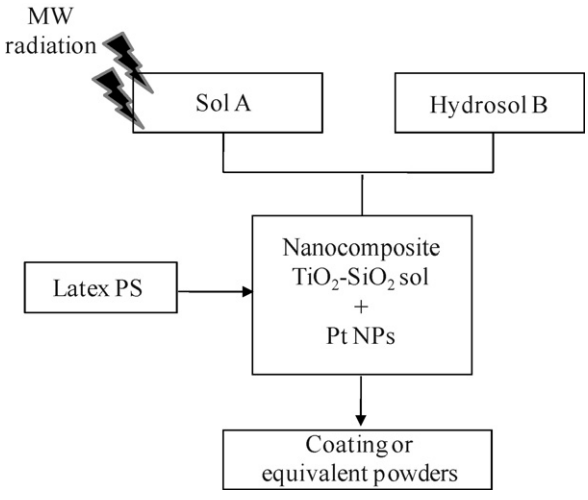

Fig. 2. Flowchart of the synthesis of TiO_2–SiO_2/Pt (80–20%) composite materials.

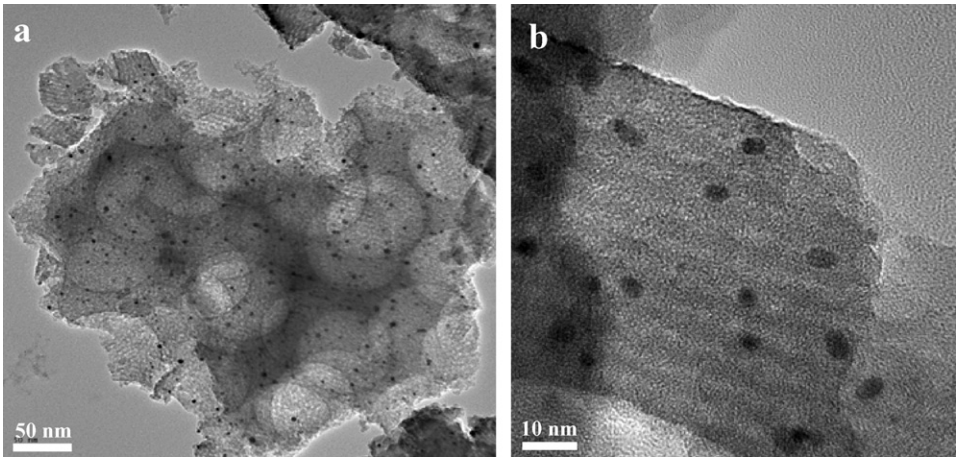

Fig. 3. TEM images of Pt/SiO_2 thin films.

(40 kV, 20 mA, λ = 1.5409 Å, 2θ varied from 20° to 75°). The crystallite sizes were estimated by applying the Scherrer equation [16] to the FWHM (full width at half maximum) of the (1 1 1) and (1 0 1) peaks of platinum and TiO_2-anatase, respectively.

N_2 adsorption–desorption isotherms were acquired using a Micromeritics ASAP 2020 instrument. The samples were previously outgassed at 200 °C for 2 h. Specific surface areas were calculated via the multi-point Brunauer–Emmett–Teller (BET) method model at relative pressures of P/P_0 = 0.06–0.3.

Finally, the permeance of single gases (He, N_2, n-C_4H_{10}, i-C_4H_{10} and SF_6) was measured through the membranes at room temperature as a function of transmembrane pressure. For these measurements the tubes, whose ends were coated with an epoxy resin, were sealed in a dead-end module with polymer o-rings. The transmembrane pressure was varied from 0.5 bar to 1.8 bar and the external pressure was atmospheric pressure. Before measurements and before changing the gas, membranes were outgassed for 2 h in vacuum at room temperature.

2.3. Catalytic activity tests

The catalytic activity for propene oxidation was measured with a reactant mixture composed of 1000 ppm C_3H_6 and 9% O_2 in He and the weight hourly space velocity (WHSV) was typically 36,000 mL g^{-1} h^{-1}. For each test, 200 mg of membrane material were introduced in a U-shaped quartz reactor. The lab-made apparatus has been already described in details elsewhere [17]. The reactor was electrically heated and the catalyst temperature was monitored using a K-type thermocouple. After the reactor was purged with He, the flow rate through the catalyst bed was fixed at 120 mL min^{-1} and the test procedure was started. The experiments were performed in a temperature-programmed way as follows: heating from room temperature to 400 °C (rate 3.5 °C/min), plateau at 400 °C for 15 min, cooling down from 400 °C to room temperature (rate 1.3 °C/min). Only the cooling step was considered for plotting the light-off curves. Reaction products were analysed by gas chromatography for N_2, C_3H_6 and CO_2. The total propene conversion (%) was calculated on the basis of propene consumption as shown in Eq. (1):

$$X = 100 \times \left(1 - \frac{[C_3H_6]_i}{[C_3H_6]_0}\right) \quad (1)$$

with i is the output rector, and 0 is the reactor entrance.

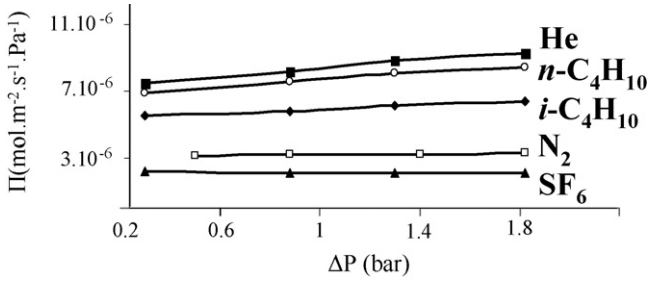

Fig. 4. Evolution of single gas permeance versus transmembrane pressure at room temperature for different gases through the HS_{pure}Pt1.7 membrane.

3. Results and discussion

3.1. Pure silica membrane materials

3.1.1. Nanostructure analysis

TEM images of the calcined HS_{pure}Pt1.7 membrane materials are shown in Fig. 3. The hierarchical structure is clearly evidenced, with macropores and ordered mesopores, as well as dispersed Pt-NPs (Fig. 3a). A higher magnification shows the location of Pt nanoparticles within the non-connected/ordered mesopores molded by the walls of the SiO_2 matrix (Fig. 3b). Most of the Pt-NPs exhibit a slightly elongated shape with an average size of ~4 nm, which perfectly fits the mesopore size measured by N_2 adsorption–desorption [14].

3.1.2. Single gas permeance measurements

The evolution of single gas permeance at room temperature through a typical HS_{pure}Pt1.7 membrane is shown in Fig. 4. The calculated ideal selectivities are close to Knudsen values, except for gas couples involving the n-C_4H_{10} and i-C_4H_{10} alkanes (Table 1). Specific adsorption and surface diffusion of alkanes on the surface of membrane pores could explain this latter result. The presence

Table 1
Calculated ideal selectivities of the HS_{pure}Pt1.7 membranes for various gas couple A/B.

$Gas_{A/B}$	α_K	α_{exp}
He/N_2	2.6	2.5
N_2/n-C_4H_{10}	1.4	0.4
N_2/i-C_4H_{10}	1.4	0.5
N_2/SF_6	2.2	1.5

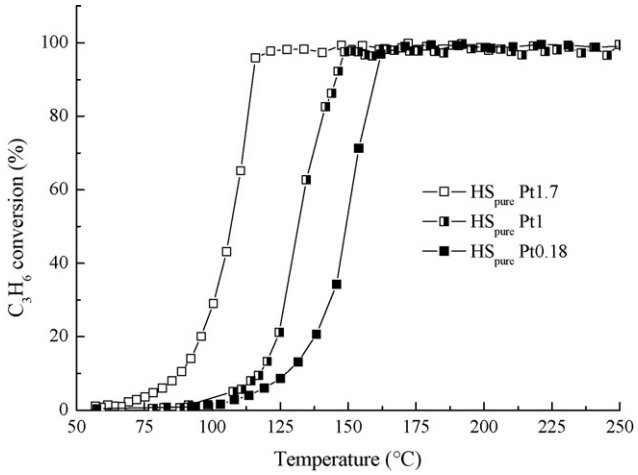

Fig. 5. Evolution of propene conversion over Pt/SiO_2 catalysts as a function of the reaction temperature.

of residual carbon after the calcination step possibly contributes to this adsorption.

3.1.3. Catalytic activity of the NPs in silica/Pt materials

The accessibility of the NPs embedded in the silica hierarchical structure was demonstrated by studying the performance of HS_{pure}Pt0.18, HS_{pure}Pt1 and HS_{pure}Pt1.7 powders for the total oxidation of propene. The evolution of the catalytic conversion of propene as a function of temperature is shown in Fig. 5. All samples exhibit attractive catalytic performance and completely convert C_3H_6 into CO_2 and H_2O at very low temperature. The catalytic activity is emphasized for the highest Pt content since the curves are shifted to lower temperatures. The light-off temperature ($T_{light\text{-}off}$, corresponding to 50% propene conversion) is measured at less than 110 °C for HS_{pure}Pt1.7, at about 125 °C for HS_{pure}Pt1 and at about 150 °C for HS_{pure}Pt0.18 sample. These light-off temperatures are quite low when compared to those obtained for classical $Pt–Al_2O_3$ catalysts with a similar Pt content [17–20]. The small and uniform size of the Pt-NPs isolated in the calibrated silica mesopores explains both their high reactivity (low $T_{light\text{-}off}$) and the relatively abrupt slope of the conversion curves (small difference between the total conversion and light-off temperatures). The presence of several big NPs in HS_{pure}Pt1.7 (≈8 nm, observed by HR-TEM) out from the mesostructured domains did not seem to alter the catalytic efficiency of this sample. On the other hand a small elongation and/or specific orientation of the Pt-NPs entrapped in the mesopores (favouring access to specific crystal faces) could possibly explain the very low $T_{light\text{-}off}$ values. The influence of both residual carbon species and support acidic properties (already assumed from the permeance measurements) could also contribute to favour propene adsorption.

These catalytic tests show that complete propene oxidation can be achieved over HS_{pure}Pt1.7 samples below 110 °C and with 100% CO_2 selectivity. The designed hierarchical structure, with embedded metal NPs, is consequently attractive in terms of both NPs accessibility and reactivity. It could be an ideal candidate for both thin-layer-supported catalysis and for catalytic membrane reactors. Such an entrapment of the catalyst in the ordered/non-connected mesopores of the hierarchical structure may be highly beneficial to the catalytic membrane properties, by avoiding NPs aggregation during long-term operation at high temperature.

3.1.4. Thermal stability of the catalytic activity

The stability of NPs is a debated requirement in relation to catalytic processes due to the well known deactivation caused by

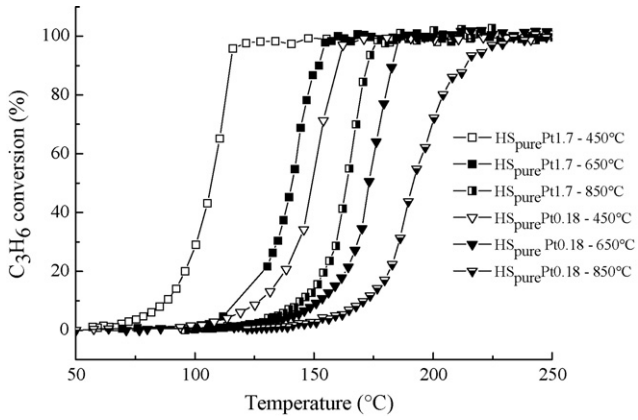

Fig. 6. Evolution of propene conversion over HS_{pure}Pt0.18 and HS_{pure}Pt1.7 catalysts calcined at 450 °C, 650 °C and 850 °C as a function of reaction temperature.

metal sintering. Therefore the influence of thermal treatments on the catalytic activity of HS_{pure}0.18 and HS_{pure}1.7 has been studied in the present work. Fig. 6 shows the evolution of the light-off curves for the total oxidation of propene for HS_{pure}Pt0.18 and HS_{pure}Pt1.7 samples after calcination at 450 °C, 650 °C or 850 °C. It is firstly observed that the total conversion occurred for all the samples at temperature lower than 200 °C which is quite low. Moreover the curve shapes still attest for the relatively monodispersity of the NP sizes, even for the highest calcination temperature and may explain these attractive results.

The sample performance in term of $T_{light\text{-}off}$ are reported in the histogram of Fig. 7, as well as the mean diameter of the corresponding Pt-NPs (determined from the FWHM of the XRD main peak at $2\theta = 39.6°$ and not shown here). Due to the low Pt content in the HS_{pure}0.18 powder, the Pt diffraction peaks were not detected and the mean Pt-NP diameter was only calculated for the HS_{pure}Pt1.7 sample. These values increase with the calcination temperature: 4 nm, 5 nm and 9 nm, for 450 °C, 650 °C and 850 °C, respectively. It is interesting to note that HS_{pure}Pt1.7 calcined at 850 °C contains relatively big Pt-NPs (∼9 nm), but is still an attractive catalyst which can convert C_3H_6 at low temperature (<160 °C). The initial localization of the metal NPs mainly inside the ordered and isolated mesopores seems to inhibit the agglomeration (sintering) of nanoparticles even after high temperature treatments up to 850 °C.

In order to better understand the above results, N_2 adsorption–desorption isotherms of the HS_{pure}Pt1.7 samples, calcined at 450 °C, 650 °C or 850 °C have been recorded (Fig. 8a). The calculated S_{BET} and associated $T_{light\text{-}off}$ values are reported in Fig. 8b. All samples show type-IV isotherms, which are repre-

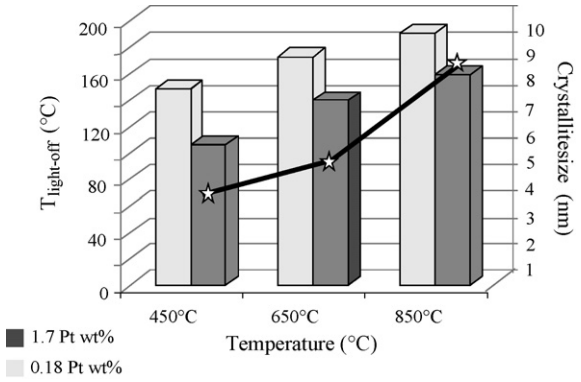

Fig. 7. Comparison of $T_{ligh\text{-}off}$ values for the total oxidation of proprene (histogram) and evolution of the Pt crystallite size (curve) for HS_{pure}Pt0.18 and HS_{pure}Pt1.7 catalysts as a function of the initial calcination temperature.

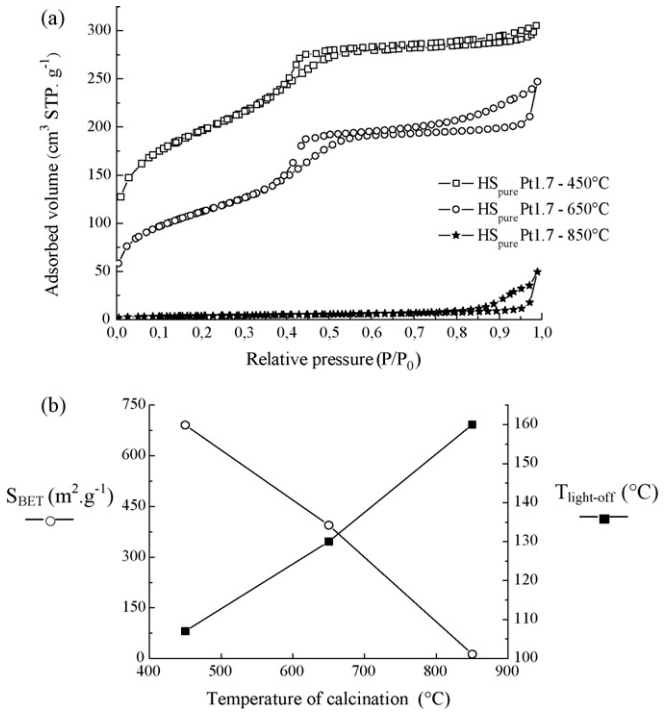

Fig. 8. N_2 adsorption–desorption isotherms of the HS_{pure}Pt1.7 samples calcined at (i) 450 °C, (ii) 650 °C or (iii) 850 °C (a), and corresponding evolution of S_{BET} and $T_{light\text{-}off}$ as a function of the calcination temperature (b).

Table 2
Porosity characteristics of the HS_{pure}Pt1.7 samples calcined at 450 °C, 650 °C and 850 °C respectively.

Temperature (°C)	S_{BET} (m^2/g)	V_{pore} (cm^3/g)	Pore diameter (nm)
450	680	0.47	4.0
650	394	0.39	3.9
850	20	0.08	2.7

sentative of mesoporous solids. The main porous characteristics of each sample are also given in Table 2. As previously observed [14], large microporosity and mesoporosity are observed for the sample treated at 450 °C. However, the third level (i.e. the macroporosity) is not here clearly detected. It is due to the fact that the experimentally investigated range of relative pressure did not reach the very high values required for capillary condensation inside the macropores. For the sample calcined at 650 °C, although a decrease of the pore volume is observed, the isotherm shape remains almost unchanged. In agreement with a significant

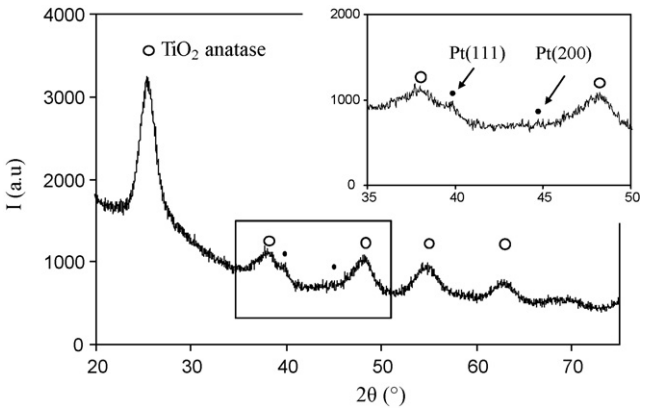

Fig. 9. Wide-angle XRD pattern of the HS_{mix}Pt1.7 sample calcined at 450 °C.

decrease of the microporosity, the specific surface area decreases from 680 $m^2\,g^{-1}$ to 394 $m^2\,g^{-1}$. After calcination at 850 °C, the hierarchical porous structure collapses and the specific surface area is strongly reduced (~20 $m^2\,g^{-1}$). The rather good catalytic performance of the sample calcined at 850 °C could be explained by the very good initial homogeneous dispersion of the Pt-NPs and by their progressive migration at the surface of the residual porosity during the densification process resulting from the calcination at high temperature.

3.2. Nanocomposite SiO_2–TiO_2-based membrane materials – influence of the oxide matrix

3.2.1. Nanostructure analysis

Fig. 9 shows the wide-angle XRD pattern of a HS_{mix}Pt1.7 unsupported membrane calcined at 450 °C. The sample exhibits four distinct peaks assigned to TiO_2-anatase (JCPDF 89-4121). The average TiO_2-anatase crystallite size was approximately 6.5 nm, as estimated from the peak width of the anatase (1 0 1) reflection by using the Scherrer equation with a spherical particle shape model for approximation. Such nanocrystalline wall structure is compatible with the formation of an ordered mesoporosity [15]. Close examination of the XRD pattern reveals that two weak but resolvable peaks can be attributed to the (1 1 1) and (2 0 0) reflections of Pt^0 (JCPDF 88-2343). These weak peaks are also broad, revealing the nanocrystalline nature of the Pt particles encapsulated in the films.

The TEM analyses allow observing the metal NPs nested in the TiO_2–SiO_2 nanocomposite phase (Fig. 10a). The smallest metal nanoparticles exhibit a mean size around 2–4 nm, with some bigger particles around 7–8 nm (Fig. 10b).

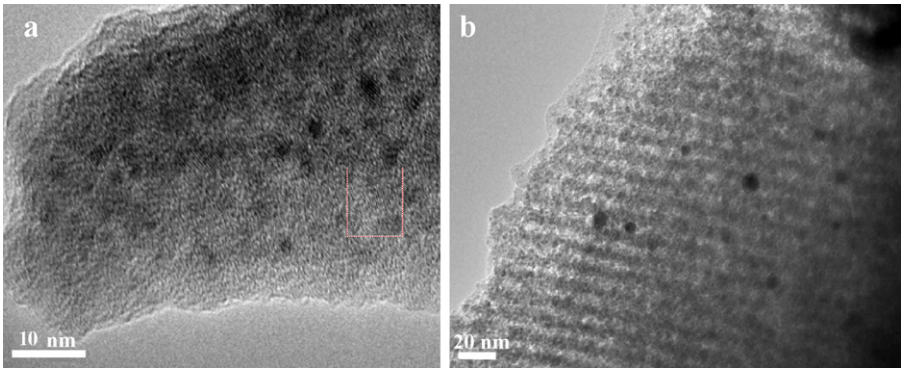

Fig. 10. TEM images of a HS_{mix}Pt1.7 thin film.

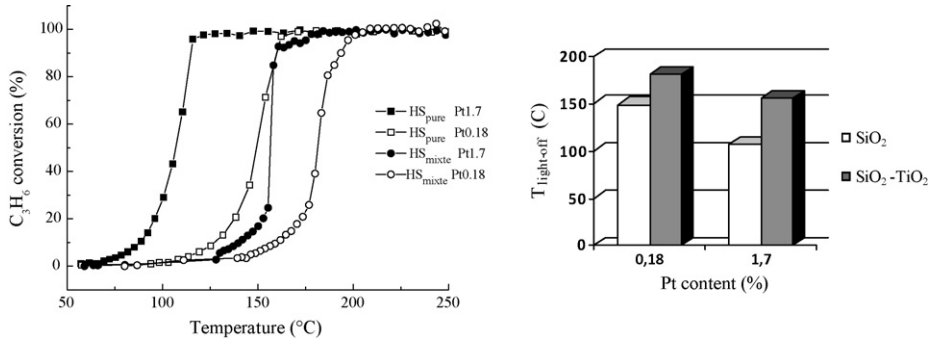

Fig. 11. Propene conversion curves and associated histograms for HS_{pure}Pt1.7, HS_{pure}Pt0.18, HS_{mix}Pt1.7 and HS_{mix}Pt0.18 samples calcined at 450 °C.

3.2.2. Influence of the type of oxide matrix on the catalytic activity of the composite materials

Fig. 11 illustrates the influence of the type of oxide matrix on the catalytic activity of HS_{pure}Pt0.18, HS_{pure}Pt1.7, HS_{mix}Pt0.18 and HS_{mix}Pt1.7 samples calcined in air at 450 °C, for the total oxidation of propene. In all cases, the shape of conversion curves reflects the relative monodispersity of the Pt-NPs. As expected, the catalytic activity increases with the Pt concentration. The following order is observed for the catalytic activity of the tested samples: HS_{mix}Pt0.18 < HS_{mix}Pt1.7 < HS_{pure}Pt0.18 < HS_{pure}Pt1.7. The associated $T_{light\text{-}off}$ values are 181 °C, 156 °C, 149 °C and 110 °C, respectively. Although the conversion of propene with the TiO_2–SiO_2 material is achieved at relatively low temperatures ($T_{light\text{-}off} \leq 180$ °C) compared to the literature data for more classical materials ($T_{light\text{-}off} > 200$ °C) [21–23], the catalytic performance of the samples with a TiO_2-based matrix is lower than that with a pure silica matrix. No positive effect is here observed due to the presence of a semi-conducting oxide in the support phase [24]. Another factor that could explain the decrease in performance is related to a higher content of chlorine in the support phase, resulting from HCl required during the TiO_2 hydrosol synthesis. Chlorine is indeed known to strongly inhibit the oxidation reactions for hydrocarbons like propane or propene. Several authors have highlighted a gap of $T_{light\text{-}off}$ up to 120 °C (depending on the type of reaction) with or without chlorine [25]. The replacement of HCl by HNO_3 in the synthesis procedure is a possible alternative strategy currently considered in our group.

4. Conclusion

A novel approach is proposed in this work for designing original multifunctional SiO_2 and SiO_2–TiO_2-based membranes containing a dispersion of accessible and very active platinum NPs. Such hierarchical structures, made by a scalable processing sol–gel method offer a promising approach to improve the accessibility, the stability and efficiency of active sites in catalytic membrane contactors. The initial localization of the Pt-NPs, mainly within the ordered and isolated mesopores of the hierarchical structure, clearly inhibits their agglomeration when exposed to aggressive (thermal) conditions. Such entrapment of the catalyst in calibrated mesopores, which could be extended to other metal/oxide systems and reactions, may be highly beneficial to the catalytic membrane performance and properties, during long-term operation at high temperature.

Acknowledgements

The authors sincerely acknowledge Dr. P. Lacroix-Desmazes (ICG, Montpellier, France) for his decisive contribution in PS latex synthesis, as well as L. Datas (CIRIMAT, Toulouse, France) for TEM analyses.

References

[1] A. Julbe, D. Farrusseng, C. Guizard, Porous ceramic membranes for catalytic reactor – overview and news ideas, J. Membr. Sci. 181 (2001) 3–20.
[2] A. Julbe, V. Rouessac, J. Durand, A. Ayral, New approaches in the design of ceramic and hybrid Membranes, J. Membr. Sci. 316 (2008) 176–185.
[3] C. Yacou, M.L. Fontaine, A. Ayral, P. Lacroix-Desmazes, P.A. Albouy, A. Julbe, One pot synthesis of hierarchical porous silica membrane material with dispersed Pt nanoparticles using a microwave-assisted sol–gel route, J. Mater. Chem. 18 (2008) 4274–4279.
[4] B.C. Bonekamp, Preparation of asymmetric ceramic membrane supports by dip-coating, in: A.J. Burggraaf, L. Cot (Eds.), Fundamentals of Inorganic Membrane Science and Technology, Elsevier, Amsterdam, 1996, pp. 141–225 (Chapter 6).
[5] G. Cortial, M. Siutkowski, F. Goettmann, A. Moores, C. Boissière, D. Grosso, P. Le Floch, C. Sanchez, Metallic nanoparticles hosted in mesoporous oxide thin films for catalytic applications, Small 2 (2006) 1042–1045.
[6] A. Mastalir, B. Rac, Z. Kiraly, G. Tasi, A. Molnar, Preparation of monodispersed Pt nanoparticles in MCM-41catalytic applications, Catal. Commun. 9 (2008) 762–768.
[7] A. Taguchi, F. Schüth, Ordered mesoporous materials in catalysis, Micropor. Mesopor. Mater. 77 (2005) 1–45.
[8] R.G. Derwent, M.E. Jenkin, S.M. Saunder, Photochemical ozone creation potentials for a large number of reactive hydrocarbons under European conditions, Atmos. Environ. 30 (1996) 181–199.
[9] P. Papaefthimiou, T. Ionnides, X.E. Verykios, Combustion of non-halogenated volatile organic compounds over group VIII metal catalysts, Appl. Catal. 13 (1997) 175–184.
[10] J.A. Moulijn, A.E. van Diepen, F. Kapteijn, Catalyst deactivation: is it predictable? What to do? Appl. Catal. A: Gen. 212 (2001) 3–16.
[11] M. Malenosvka, S. Martinez, M. Neouze, U. Schubert, Growth of metal nanoparticles in a sol–gel silica thin film, Eur. J. Inorg. Chem. (2007) 2609–2611.
[12] S.J. Tauster, S.C. Fung, R.L. Garten, Strong metal–support interactions. Group 8 noble metals support on TiO_2, J. Am. Chem. Soc. 100 (1978) 170–175.
[13] X. Zhang, H. Yang, F. Zhang, K.Y. Chan, Preparation and characterization of Pt–TiO_2–SiO_2 mesoporous materials and visible-light photocatalytic performance, Mater. Lett. 61 (2007) 2231–2234.
[14] C. Yacou, A. Ayral, A. Giroir-Fendler, M.L. Fontaine, A. Julbe, Hierarchical porous silica membranes with dispersed Pt nanoparticles, Micropor. Mesopor. Mater. 26 (2009) 222–227.
[15] F. Bosc, A. Ayral, P.A. Albouy, C. Guizard, A simple route for low-temperature synthesis of mesoporous and nanocrystalline anatase, Thin Films Chem. Mater. 15 (2003) 2463–2468.
[16] P. Scherrer, Estimation of the size and internal structure of colloidal particles by means of Roentgen X-rays, Nachr. Ges. Wiss. Gottingen 2 (1918) 98–112.
[17] P. Denton, A. Giroir-Fendler, H. Praliaud, M. Primet, Role of the nature of the support (alumina or silica), of the support porosity, and of the Pt dispersion in the selective reduction of NO by C_3H_6 under lean-burn conditions, J. Catal. 189 (2000) 410–420.
[18] A. Chiba, M. Komoda, T. Kosumi, N. Nanba, N. Azuma, A. Ueno, Difference in catalytic combustion of propane and propene on Pt/Al_2O_3 catalyst, Chem. Lett. 8 (1999) 801–802.
[19] S. Aouad, E. Saab, E. Abi Aad, A. Aboukaïs, Reactivity of Ru-based catalysts in the oxidation of propene and carbon black, Catal. Today 119 (2007) 273–277.
[20] M. Labaki, S. Siffert, J.F. Lamonier, E. Zhilinskaya, A. Abouka, Total oxidation of propene and toluene in the presence of zirconia doped by copper and yttrium: role of anionic vacancies, Appl. Catal. B: Environ. 43 (2003) 261–271.
[21] A.C. Gluhoi, N. Bogdanchikova, B.E. Nieuwenhuys, The effect of different types of additives on the catalytic activity of Au/Al_2O_3 in propene total oxidation: transition metal oxides and ceria, J. Catal. 229 (2005) 154–162.
[22] M. Hosseini, S. Siffert, H.L. Tidahy, R. Cousin, J.F. Lamonier, A. Aboukais, A. Vantomme, M. Roussel, B.L. Su, Promotional effect of gold added to palladium

supported on a new mesoporous TiO_2 for total oxidation of volatile organic compounds, Catal. Today 122 (2007) 391– 396.
[23] M. Lamallem, R. Cousin, R. Thomas, S. Siffert, F. Aïssi, A. Aboukaïs, Investigation of the effect of support thermal treatment on gold-based catalysts activity towards propene total oxidation, C. R. Chimie 12 (2009) 772– 778.
[24] S.J. Tauster, Strong metal–support interaction, Acc. Chem. Res. 20 (1987) 389–394.
[25] F.J. Gracia, J.T. Miller, A.J. Kropf, E.E. Wolf, Kinetics, FTIR, and controlled atmosphere EXAFS study of the effect of chlorine on Pt-supported catalysts during oxidation reactions, J. Catal. 209 (2002) 341–354.